Molecular Syndromology

Novel Insights from Clinical Practice

Mol Syndromol 2023;14:347–361
DOI: 10.1159/000529306

Received: June 29, 2022
Accepted: January 22, 2023
Published online: April 12, 2023

Expanding the p.(Arg85Trp) Variant-Specific Phenotype of HNF4A: Features of Glycogen Storage Disease, Liver Cirrhosis, Impaired Mitochondrial Function, and Glomerular Changes

Mara Grassi[a] Bernard Laubscher[b, c] Amit V. Pandey[a, d] Sibylle Tschumi[e] Franziska Graber[f] André Schaller[g] Marco Janner[a] Daniel Aeberli[h] Ekkehard Hewer[f, i] Jean-Marc Nuoffer[a, j] Matthias Gautschi[a, j]

[a]Pediatric Endocrinology, Diabetology and Metabolism, Department of Pediatrics, Inselspital, University Hospital Bern, University of Bern, Bern, Switzerland; [b]Department of Pediatrics, Réseau hospitalier neuchâtelois, Neuchâtel, Switzerland; [c]Department of Pediatrics, Lausanne University Hospital, University of Lausanne, Lausanne, Switzerland; [d]Department of Biomedical Research, University of Bern, Bern, Switzerland; [e]Pediatric Nephrology, Inselspital, University Hospital Bern, Bern, Switzerland; [f]Institute of Pathology, University of Bern, Bern, Switzerland; [g]Department of Human Genetics, Inselspital, University Hospital Bern, University of Bern, Bern, Switzerland; [h]Department of Rheumatology and Immunology, Inselspital, University Hospital Bern, Bern, Switzerland; [i]Institute of Pathology, Lausanne, University Hospital and University of Lausanne, Lausanne, Switzerland; [j]Institute of Clinical Chemistry, Inselspital, University Hospital Bern, University of Bern, Bern, Switzerland

Established Facts

- The p.(Arg85Trp) variant of HNF4α causes a complex phenotype affecting not only the pancreas but also the liver and kidneys. Few details were known.
- Animal models suggest the involvement of mitochondria in the pathogenesis of this variant-specific phenotype.

Novel Insights

- This case expands the p.(Arg85Trp) variant phenotype of HNF4A by adding in detail features of glycogen storage disease, liver cirrhosis, impaired mitochondrial function, and glomerular changes.
- We describe abnormalities of mitochondrial structure and function in the context of human pathology.

Keywords
HNF4A · Hyperinsulinism · Renal Fanconi syndrome · Hepatopathy · Mitochondria

Abstract
Introduction: The p.(Arg85Trp) variant-specific phenotype of hepatocyte nuclear factor 4 alpha shows a complex clinical picture affecting three different organ systems and their corresponding metabolisms. Little is known about the mo-

Karger@karger.com
www.karger.com/msy

Correspondence to:
Matthias Gautschi, matthias.gautschi@insel.ch

lecular mechanisms involved and their relationship with the diverse symptoms seen in the context of this specific variant. Here, we present data of a new patient that expand the clinical phenotype, suggesting possible disease mechanisms. ***Case Presentation:*** Clinical data were extracted from the patient's charts. The liver, kidney, and muscle were analyzed with routine histology and electron microscopy. Mitochondrial function was assessed by respirometric analyses and enzymatic activity assays. Structure and sequence analyses of this specific variant were investigated by in silico analyses. Our patient showed the known features of the variant-specific phenotype, including macrosomia, congenital hyperinsulinism, transient hepatomegaly, and renal Fanconi syndrome. In addition to that, she showed liver cirrhosis, chronic kidney failure, and altered mitochondrial morphology and function. The clinical and biochemical phenotype had features of a new type of glycogen storage disease. ***Discussion:*** This case expands the p.(Arg85Trp) variant-specific phenotype. Possible pathomechanistic explanations for the documented multiorgan involvement and changes of symptoms and signs during development of this ultra-rare but instructive disorder are discussed.

Introduction

Hepatocyte nuclear factor 4 alpha (HNF4α) is a transcription factor (TF) critically involved in the determination and maintenance of cell and tissue identity and it is mainly expressed in the liver, proximal tubule of the kidney, pancreas, and gastrointestinal tract. HNF4α contains a cysteine zinc finger DNA-binding domain (DBD), a lipophilic ligand-binding domain (LBD), and additional domains with activation function (AF-1 and AF-2) [Chandra et al., 2013]. Together with other TFs, HNF4α is integrated into complex autoregulatory and cross-regulatory networks, which are dynamic in a time- and tissue-specific manner. They orchestrate gene programs, depending on dimerization (homo- vs. heterodimers), the presence of co-activators or corepressors, the type of tissue, and the cell stage [Lau et al., 2018].

The *HNF4A* gene is on chromosome 20q13.12, and expression is regulated by two different promoters (P1 and P2) [Thomas et al., 2001]. Different promoter usage and alternative splicing generate 12 functionally different isoforms of HNF4α [Babeu and Boudreau, 2014; Lau et al., 2018]. While HNF4α functions exclusively as a homodimer, functional diversity is created by the expression and combination of different isoforms. In the liver and kidneys, P2 is active during embryonic life, whereas P1 is predominant in the adult organs. In the pancreas, it is the other way round. In the adult gut, both promoters are active [Harries et al., 2008].

Most of our knowledge about TF function and regulation during development and adulthood has been gained from rodents (reviewed by Lau et al. [2018]). However, important aspects of human molecular physiology and pathology differ considerably from rodents. Thus, inactivating variants, leading to loss of function and/or haploinsufficiency, result in maturity-onset diabetes of the young type 1 (MODY1) in humans [Lausen et al., 2000; Ferrer, 2002]. It may be accompanied by mild changes of lipid metabolism in the liver of adult patients [Pearson et al., 2005], as well as by macrosomia and hyperinsulinaemic hypoglycaemia in newborns [Pearson et al., 2007].

Hamilton et al. [2014] recognized that the heterozygous p.(Arg85Trp) (c.253C>T; NM_000457.5) (also reported as p.R63W [c.187C>T; NM_175914.4] or p.R76W [c.232C>T NM_001287182.2]) variant of *HNF4A* leads to a specific phenotype affecting three different organ systems: the pancreas, kidneys, and liver, also causing hepatomegaly with increased glycogen content in the liver and a Fanconi-type proximal tubulopathy [Hamilton et al., 2014]. The arginine at position 85 appears to be central to the specificity of the DNA-binding motif exclusively recognized by HNF4α; loss of this amino acid may lead to a change in the binding profile [Fang et al., 2012]. Consequently, the set of target genes activated by HNF4α may be altered, leading to a dominant negative or gain-of-function effect. In drosophila, this variant was found to produce non-genomic effects including mitochondrial dysfunction and cytosolic aggregation [Marchesin et al., 2019]. However, it is not excluded that a loss of function may lead to unstable or reduced cell differentiation with decreased expression of tissue proteins, e.g., in the proximal tubules of the kidneys or to a combination of these hypothetical effects (e.g., reviewed by Lemaire [2021]). So far, we do not know. Thus, human pathology can be instructive.

Here, we present a new case that expands the clinical and biochemical phenotype and may give some insight into the pathomechanisms of this specific *HNF4A* variant. In addition to the known classical clinical findings described previously, our patient presents not yet reported clinical and biochemical aspects of this variant-specific phenotype, including mitochondrial impairment, lipoprotein metabolism, liver injury, and renal dysfunction. With the data of our case, we take a hypothesis-generating approach on three different levels (molecular, organ, and metabolism), which will need further basic and clinical research.

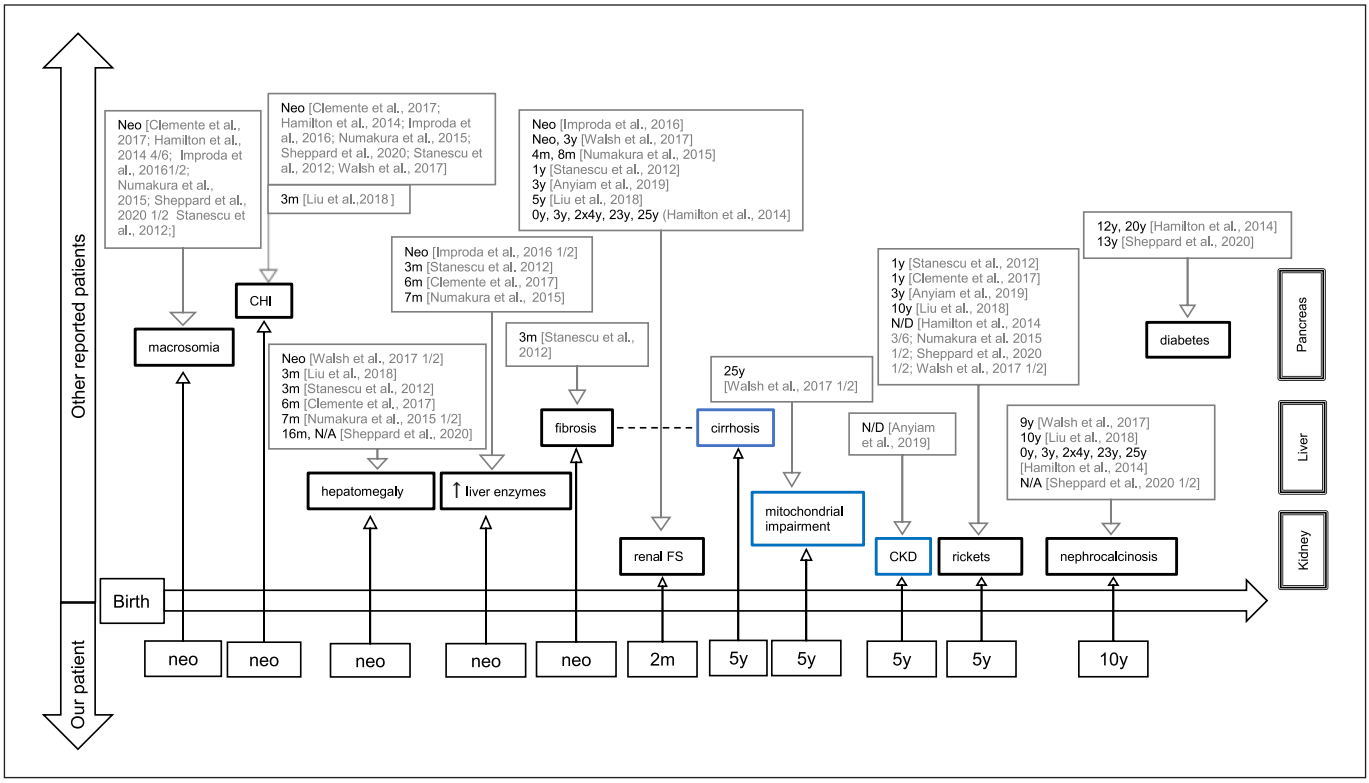

Fig. 1. Timeline illustrating the time of occurrence of the different symptoms. It compares the other reported cases (upper half) with our case (lower half) and is divided into the three affected organs (e.g., the pancreas, liver, kidney). Marked in blue: clinical features of the patient expanding the phenotype. neo, neonatal (0–28 days); m, months; y, years; CHI, congenital hyperinsulinism; CKD, chronic kidney disease; x/y, number of affected patient/all reported patients, if not specified otherwise, it affects all reported patients; ND, no data regarding age of occurrence.

Case Report

The case history and routine biochemical analyses were extracted from the patient's charts. Figure 1 shows the occurrence of different symptoms and signs of this case compared to cases of the literature. The timeline of the different treatments is summarized in Figure 2.

The girl was born after an uneventful pregnancy at 38 weeks of gestation, to nonconsanguineous parents of Caucasian ancestry. At birth, she was macrosomic with a birth weight of 4,230 g (centile >90th, Z score +2.4), length of 53 cm (centile >90th, Z score +2.1), and head circumference of 37 cm (centile >90th, Z score +2.3). At 8 minutes of life, she started to show bouts of severe trembling associated with profound hypoglycemia and was transferred to the neonatal intermediate care unit. With an increased insulin level (43.2 mU/L [5–18mU/L]) in hypoglycemia (1.1mmol/L) and physiological levels of growth hormone and cortisol, hyperinsulinism was diagnosed on the second day of life. During the first 10 days, hyperinsulinism was difficult to manage as she showed hypo- as well as hyperglycemic periods with treatment of G10–20% perfusions, fractionated enteral feeding with 8 meals per day, and diazoxide. Afterward, she showed a stable glycemic profile with glucose levels between 3.1 mmol/L and 5.7 mmol/L during the hospital stay. Transient neonatal cholestasis was treated with ursodeoxycholic acid during the first year of life.

Follow-up included abdominal ultrasound from age 2 weeks to rule out biliary atresia. At age 2 months, it showed hepatomegaly and diffuse micronodular lesions throughout the entire liver parenchyma, which remained stable during the following years. From the age of 3 weeks on, the patient showed features of renal Fanconi syndrome with loss of electrolytes, glucosuria, aminoaciduria, and loss of low-weight proteins. This was initially interpreted as a side effect of diazoxide. In addition, she presented an organic aciduria, with intermittent increase of lactate and intermediates of the Krebs cycle (fumarate, malate, and 2-oxoglutarate, data not shown).

During the first months of life, she had poor weight gain. After 1 year, her weight stabilized between centiles 10–25. After a transitory language delay, the patient's developmental milestones were acquired normally.

At the age of 3 years, the addition of bicarbonate therapy was initiated to counteract the metabolic acidosis caused by the proximal tubulopathy. During follow-up, electrolyte loss through the proximal tubulopathy increased, and at the age of 4 years, she started showing signs of chronic kidney disease (CKD), with an increase in serum creatinine and serum urea and decreased estimat-

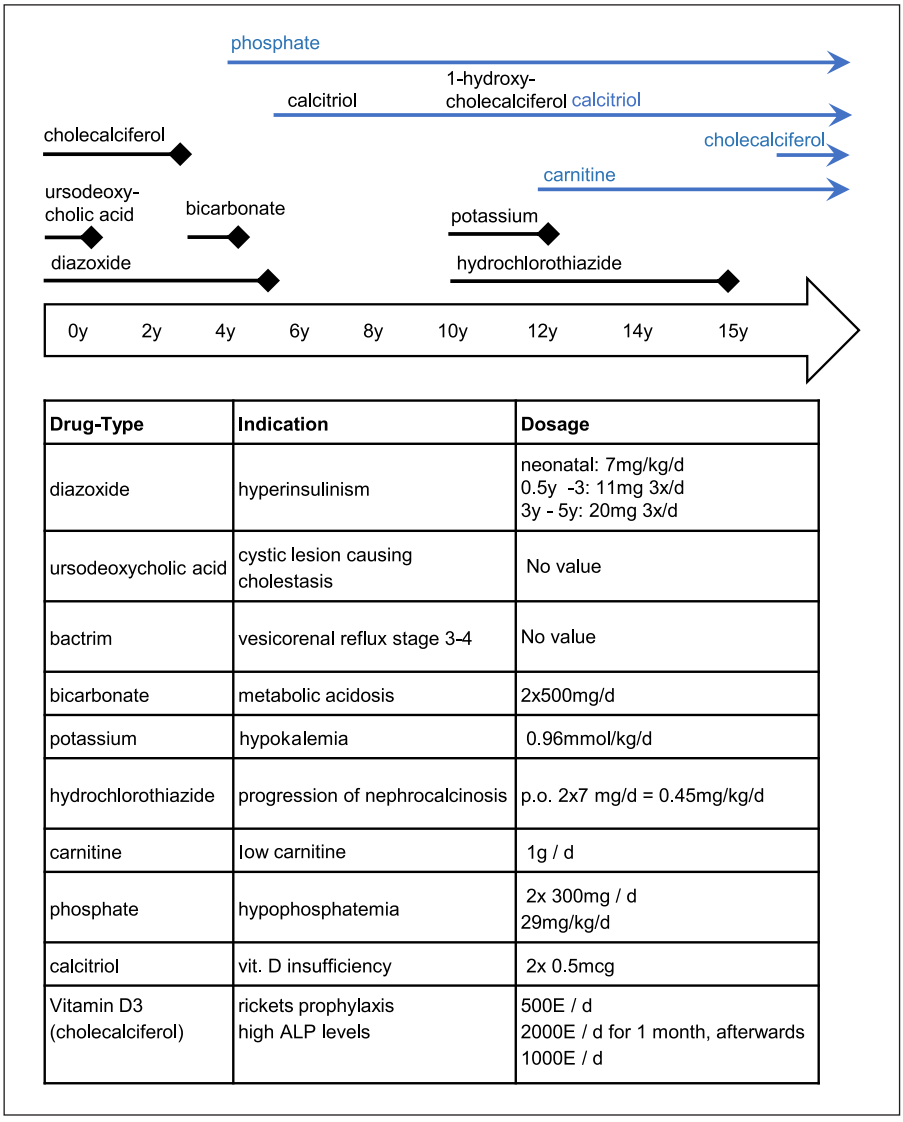

Drug-Type	Indication	Dosage
diazoxide	hyperinsulinism	neonatal: 7mg/kg/d 0.5y -3: 11mg 3x/d 3y - 5y: 20mg 3x/d
ursodeoxycholic acid	cystic lesion causing cholestasis	No value
bactrim	vesicorenal reflux stage 3-4	No value
bicarbonate	metabolic acidosis	2x500mg/d
potassium	hypokalemia	0.96mmol/kg/d
hydrochlorothiazide	progression of nephrocalcinosis	p.o. 2x7 mg/d = 0.45mg/kg/d
carnitine	low carnitine	1g / d
phosphate	hypophosphatemia	2x 300mg / d 29mg/kg/d
calcitriol	vit. D insufficiency	2x 0.5mcg
Vitamin D3 (cholecalciferol)	rickets prophylaxis high ALP levels	500E / d 2000E / d for 1 month, afterwards 1000E / d

Fig. 2. Medication of the patient in a timeline and the corresponding indications and dosages. Blue arrows = current medication.

ed glomerular filtration rate. Renal loss of phosphate was supplemented orally. Due to signs of rickets on the X-ray of the knee, she was started on calcitriol at age 5 years. Under this treatment, levels of calcium, phosphate, and parathyroid hormone, as well as bone mineral density of the lumbar spine and hip were within the normal range by the age of 8 years. The volumetric assessment of radius at 66% and 4% of total length by peripheral quantitative computed tomography showed a trabecular and cortical density in the lower normal range (Z-score: 1 SD) at 15 years [Rauch and Schönau, 2005]. Similar results were found at the lateral distal femora (25–50th centile [Zemel et al., 2009]). Alkaline phosphatase (ALP) as well as β-cross laps (CTX at age 10y: 2446 pg/mL [330–996]; at age 15.5y: 1291 pg/mL [48–579]) levels persisted at high levels. Hyperinsulinism gradually improved, and diazoxide could be stopped at age 5 years, while regular meals were continued. At physical examination, striking frontal bossing, as typically seen in patients with hepatic glycogen storage diseases, was observed. It disappeared at puberty.

Also at the age of 5 years, in the context of a change in the treating team, a complete workup for a mitochondrial disease was performed, with liver, kidney, and muscle biopsies. Fanconi-Bickel syndrome was excluded as no variant was found in the *SCL2A2* gene, and immunohistochemistry demonstrated the presence of GLUT2 on liver sections.

At age 10 years, calciuria and nephrocalcinosis led to the introduction of hydrochlorothiazide. At age 15 years, it was stopped due to the risk of long-term side effects and because CKD progressed less as the estimated glomerular filtration rate had been stable since age 10 years.

At the age of 12 years, a trio whole-exome sequencing was performed, showing a de novo p.(Arg85Trp) variant in the *HNF4A* gene. At present, at 15.5 years of age, her condition, including liver function, glucose metabolism, and proximal tubulopathy, appears to be stable under treatment with calcitriol, cholecalciferol, carnitine, and phosphate (Fig. 2).

Table 1. Biochemical features and follow-up of the patient

	Neonatal pre- diazoxide	Age 3 years on diazoxide	Age 5 years on Ph, calcitriol	Age 7 years on Ph, calcitriol	Age 10 years on Ph, calcitriol, +HCT, +K	Age 15.5 years on Ph, calcitriol, +cholecalciferol
Liver						
AST, IU/L	58 (0–82)	**59** (9–45)	**100** (<45)	**42** (<35)	35 (<35)	22 (<35)
ALT, IU/L	45 (0–57)	**58** (8–38)	**117** (<45)	**37** (<35)	28 (<35)	15 (<35)
GGT, IU/L	**733** (5–55)	**43** (6–42)	**47** (5–36)	36 (5–36)	31 (5–36)	16 (5–36)
Bilirubin total/direct, µmol/L	"increased"	"normal"	ND	9 (<17)/3 (<5)	10 (<17)/4 (<5)	9 (<17)/4 (<5)
Lipid metabolism						
Total cholesterol, mmol/L	ND	ND	**1.48** (2.89–5.00)	**2.54** (2.89–5.00)	3.44 (2.79–5.3)	4.11 (2.38–6.05)
HDL, mmol/L	ND	ND	**0.49** (>100)	**0.86** (>1.00)	1.61 (>1.04)	1.84 (>1.04)
LDL, mmol/L	ND	ND	**0.99** (<3.35)	**1.33** (<3.35)	1.73 (<3.34)	2.29 (<3.34)
LDL/HDL	ND	ND	2.02 (<4.00)	1.55 (<4.00)	**1.07** (1.7–3.1)	**1.24** (1.7–3.1)
Triglyceride, mmol/L	ND	ND	0.83 (<1.55)	0.72 (<1.55)	0.78 (<1.7)	0.63 (<1.7)
Kidney						
Glomerular function						
eGFR, mL/min/1.73m^2	ND	ND	107.9 (133±27[a])	**48** (133±27[a])	**46.7** (133±27[a])	**46.3** (126±22[a])
Creatinine, µmol/L blood	ND	**46** (27–42)	39 (<68)	**89** (<68)	**105** (<60)	**124** (45–84)
Urea, mmol/L blood	ND	6.5 (2.1–8.0)	5.1 (2.5–6.0)	**9.9** (2.5–6.0)	**11.5** (2.5–6.0)	7.4 (2.9–7.5)
Proximal tubular function						
Glucosuria (Stix)	**+++**	ND	ND	ND	**++++**	**++++**
TRP, %	ND	**73.2** (>81)	**65.8** (>81)	**70** (>81)	**59.4** (>81)	**51.6 (>81)**
Organic aciduria	**increased$^+$**	**increased^{++}**	normal	normal	**Increased$^+$**	**Increased$^+$**
Calciuria, mol/mol cr	ND	**2.87**(<1.16)	**1.74** (<0.85)	**1.58** (<0.85)	**1.42** (<0.85)	**1.49** (<0.85)
FE Mg, %	ND	ND	3.66 (3–5)	ND	**9.8** (3–5)	**11** (3–5)
FE K, %	ND	ND	5.7 (5–15)	ND	14.7 (5–15)	**31** (5–15)
FE uric acid, %	ND	ND	**40.7** (<0.6)	**36.8** (<0.6)	**50.8** (<0.4)	**48.9** (<0.4)
Albuminuria (mg/mmol cr)	ND **(Stix+)**	**56.4** (<2.5)	**42** (<2.3)	**38.53** (<2.3)	**30** (<2.3)	**17.25** (<2.3)
Tubular proteins						
RBP, mg/mmol cr	ND	ND	ND	**37.64** (<0.08)	ND	**18.61** (<0.08)
α1-Microglob, mg/mmol cr	ND	ND	ND	**121.7** (<1.58)	ND	**39.7** (<1.58)
Bone metabolism						
iPTH, pg/mL	ND	**62** (20–60)	64 (10–73)	8.3 (2.7–25)	14.7 (4.3–34)	29.4 (1.2–39)
ALP, IU/L	ND	**942** (108–317)	**919** (<300)	**481** (<300)	**630** (<300)	**268** (50–135)
25-Hydroxy-Vit D3, nmol/L	ND	74 (21–131)	53 (23–113)	**120** (23–113)	95 (50–134)	**276** (50–117)

Table illustrating results of the routine biochemical follow-up analyses shown at five different ages and structured on an organ-respective level. Representative annual values were taken from the semiannual controls. Reference values in parentheses. ND, no data; Ph, K, supplemental phosphate and potassium, respectively; HCT, hydrochlorothiazide; C, creatinine; eGFR, estimated glomerular filtration rate; iPTH, parathyroid hormone; TRP, tubular reabsorption of phosphate; FE, fractional excretion; RBP, retinol binding protein. $^{+/++}$ nonspecific slight/moderate increase of Krebs cycle intermediates. Bold, values outside reference ranges.
[a] Reference: Geary and Schaefer [2008].

Investigations

Genetics

DNA was extracted from venous blood samples, and trio-exome sequencing, using Agilent SureSelect Human All Exon v6, was performed on an Illumina instrument.

Sequence and Structure Analysis of HNF4α

For the HNF4α structure analysis, a three-dimensional crystal structure of human HNF4α from the protein structure database (PDB # 4IQR) was used. Side chains of mutated arginine were optimized by the screening of rotamer libraries [Canutescu et al., 2003] and molecular dynamics (MD) simulations using YASARA [Krieger and Vriend, 2015]. The protein structures were then subjected to 500 steps of steepest descent and simulated annealing minimizations using AMBER14 force filed and TIP3P water model [Jorgensen et al., 1983; Duan et al., 2003], followed by 1000 psi of explicit solvent MD simulations at 310 K. Structural analysis was performed after the MD simulation systems were stable. All illustrations were prepared with PyMOL (www.pymol.org) and rendered as ray-traced images using PovRay (www.povray.org).

Histology

All biopsies (skin [for fibroblast culture], liver, muscle, and kidney) were performed at 5 years of age. Samples were fixed in neutral-buffered formalin followed by paraffin embedding. Histological analyses of the liver and kidney included routine histological

Table 2. Abdominal ultrasound of the patient

	Neonatal	Age 3 years	Age 7 years	Age 10 years	Age 15 years
Liver					
Hepatomegaly	+	+	+	+	–
Micronodular changes	+	+	+	+	+
Portal hyper-echogenities	–	–	–	–	–
ARFI levels	ND	ND	ND	Normal	Normal
Bile duct walls	Hyperechoic	Thickened	Normal	Normal	Normal
Additional findings	Cystic lesion	→	Ectasia of the common bile duct		
Kidney					
Hyper-echogenities	–	–	+	+	–
Nephro-calcinosis	–	–	–	+	+
VUR	+ (2b bilateral)	–	–	–	–
Additional findings					Few cortical cysts (left side)

Table summarizing results of the regular abdominal ultrasound at five different ages. ARFI, acoustic radiation force impulse imaging; VUR 2b, vesicoureteral reflux grade 2b; ND, no data.

staining and direct immunofluorescence on cryostat samples. Histological analyses of the muscle included enzyme histochemistry performed on the cryostat section of the muscle biopsy.

Samples of the liver and the kidney were processed for electron microscopy by fixation in a solution of 3% glutaraldehyde in 0.1 M potassium phosphate buffer followed by a solution of 1% osmium tetroxide in 0.1 M sodium cacodylate buffer. After dehydration in increasing concentrations of ethanol, the specimens were passed through acetone and embedded in Epon (Sigma-Aldrich). Ultrathin sections (70 nm) were cut and double-stained with UranyLess (Delta Microscopies, Frances) and 3% lead citrate. Electron micrographs were taken on a Morgagni M268 Electron Microscope with an SIS Morada Camera.

Mitochondrial Function

Mitochondrial enzymatic activities of the skeletal muscle homogenates and isolated mitochondria of fibroblasts were performed as described previously [Schaller et al., 2011]. The activities of the individual respiratory chain complexes and the mitochondrial matrix enzyme citrate synthase were measured spectrophotometrically in a UV-1601 (Shimadzu, Kyoto Japan) in 1-mL sample cuvettes maintained at 30°C as described by Shepherd and Garland [1969].

Oxygen consumption in permeabilized muscle fibers was determined at 37°C using the OROBOROS oxygraph (Innsbruck, Austria). Muscle fibers were resuspended in Mitochondrial Respiration Medium MiR05 [Renner et al., 2003] and permeabilized by digitonin (10 µg/106 cells). The rates of respiration (expressed in pmol O2 s^{-1} 10^{-6} cells) were determined in the presence of 2 mM ADP and different combinations of substrates and inhibitors: 10 mM pyruvate/2 mM malate; 10 mM succinate/0.5 mM rotenone; 4 mM ascorbate/0.5 mM TMPD. Measurements of oxygen consumption by ascorbate/TMPD (tetramethyl-p-phenylenediamine) represent KCN (1 mM)-sensitive values in the presence of 12.5 mM antimycin A; maximal respiration was determined after adding FCCP, and respiratory control ratios calculated as described by Gnaiger [2020].

Findings

Routine Investigations

The biochemical features of the patient are summarized in Table 1. Liver enzymes increased during early childhood and decreased afterward to normalize by age 10 years. Transitory neonatal cholestasis resolved within a few weeks. Initially, the patient had low levels of LDL and HDL, a low level of total cholesterol, and normal triglyceride levels. The HDL levels increased to a normal level at around 8 years of age. During the entire follow-up, LDL and total cholesterol levels steadily increased, too. At age 15 years, apolipoprotein levels (ApoA1, ApoA2, and ApoB) were normal (data not shown).

The loss of glucose, low-molecular-weight proteins, amino acids, calcium, phosphate, and other electrolytes due to proximal tubulopathy gradually increased during early childhood to maximum levels at around 5 to 7 years of age. The differential analysis of urinary proteins showed mixed proteinuria, of mainly tubular origin (data not shown).

The main findings of the abdominal ultrasound are summarized in Table 2. Heterogenous micronodular lesions of the liver parenchyma were present during the neonatal period and remained stationary during follow-up. Acoustic radiation force impulse imaging values remained normal during the whole follow-up. Hepatomegaly was detected at neonatal age and entirely resolved by the age of 15.5 years.

At age 5 years, hyperechogenicities in the renal parenchyma among the medullary pyramids were detected as a sign of tubulopathy. At age 10 years, medullary nephrocalcinosis was detected. During follow-up, it did not progress and kidney growth was normal, with a successive normalization of neonatal nephromegaly.

Molecular Genetics

Trio-whole-exome sequencing showed a de novo, pathogenic variant [Stanescu et al., 2012; Hamilton et al., 2014; Numakura et al., 2015; Improda et al., 2016], c.187C>T, p.(R85W) in *HNF4A*. In addition to automated bioinformatic analysis, the data were scanned manually for potentially relevant variants. No other genetic defect was identified.

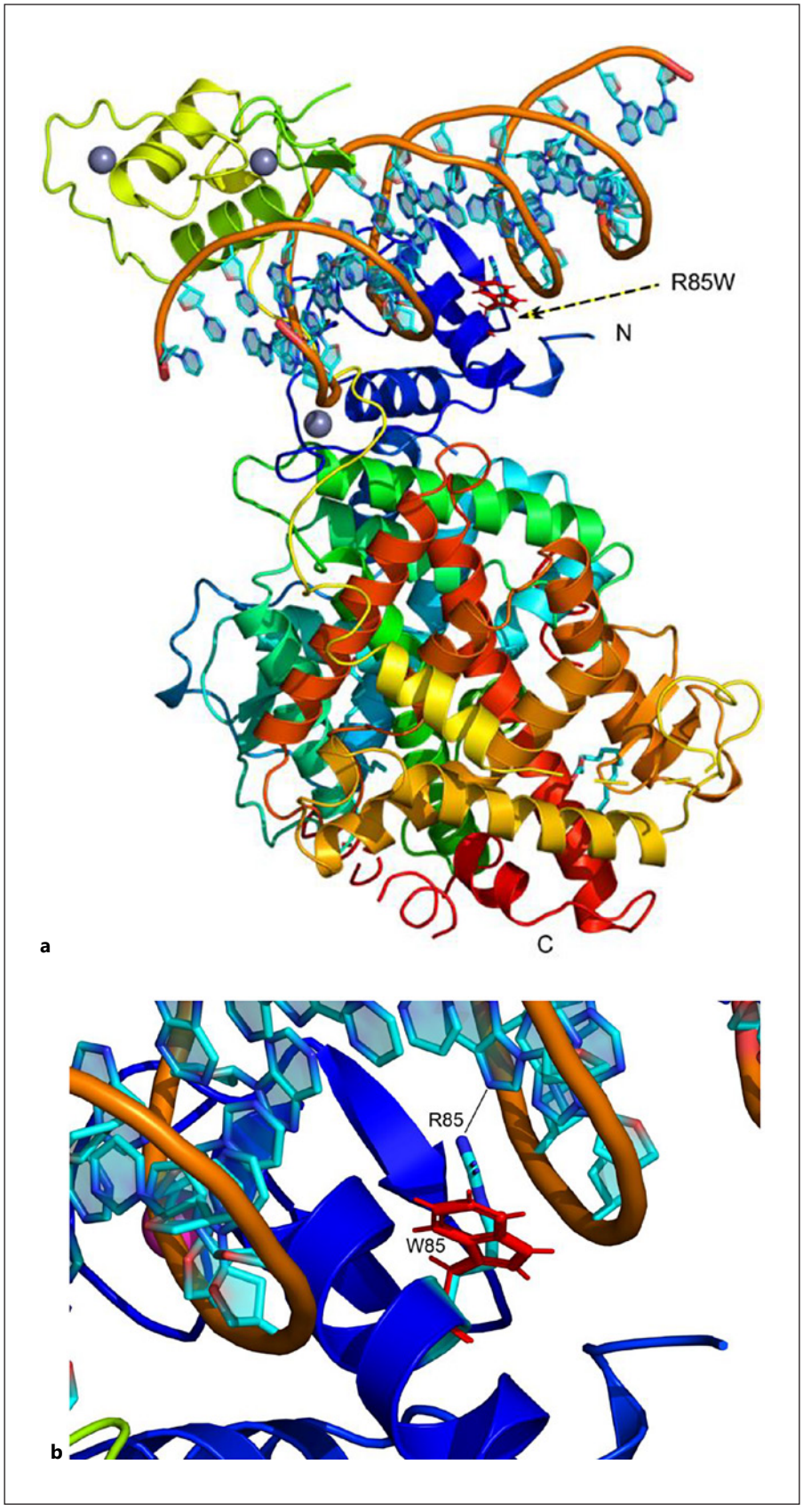

Fig. 3. a Model of HNF4α showing the alignment of WT and p.Arg85Trp (R85W) variant structures. The structure is shown as a ribbons model colored in the rainbow from the amino terminus to the carboxy terminus. The arginine 85 residue is located in DBD and is part of the DNR interaction site in HNF4α. Protein structure models were generated based on the crystal structure of HNF4α from the protein structure database (PDB # 4IQR) using in silico mutagenesis. **b** Close-up of the HNF4α structure. The WT (Arg85) and mutated (Trp85) structures were aligned and superimposed to show the differences. The WT residue is in natural elemental colors and mutated tryptophan is shown in red. A black line shows the interaction with a guanidine residue of the DNR1 half-site (AACTAGGTCAAAGGTCA). The variant of arginine 85 to tryptophan is predicted to break the interactions with DNRs and destabilize the overall structure.

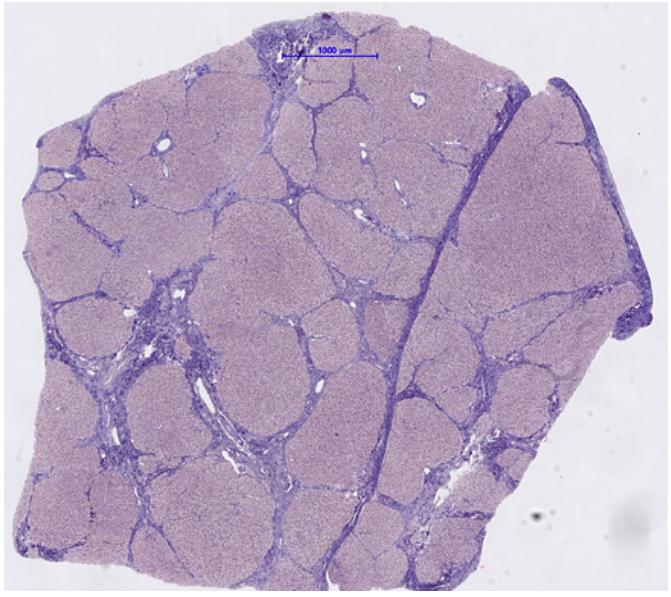

Fig. 4. Liver histology from biopsies performed at age 5 years. Methods: Samples were fixed in paraformaldehyde followed by paraffin embedding and routine histological staining. Results: Liver histology showing complete porto-portal bridging cirrhosis and limited inflammation among the portal fields and septa. The shape of some hepatocytes was described as slightly rounded. Increased deposits of glycogen were also seen.

Sequence and Structure Analysis of HNF4α

We used a standard DNA response element with a direct repeat of AGGTCA half-sites with one base-pair spacing (DR1, AACTAGGTCAAAGGTCA). DR1 is considered the major consensus binding site for HNF4α [Wallerman et al., 2009]. In the dimeric form of HNF4α crystal structure, the two DBDs are near AGGTCA half-sites of DNR1, and interactions with the major grooves of DNA and DBD were observed (Fig. 3). Due to the asymmetric nature of the HNF4α homodimer, the different parts of DNR1 half sites can be seen to interact with two different molecules of the HNF4α, as previously shown [Fang et al., 2012]. Moreover, the arginine 85 residue is near serine 87, whose phosphorylation by protein kinase c (PKC) is linked to a negative impact on DNA binding by changing the optimal positioning of HNF4α LBD and DBD. A similar structural change can be predicted by the introduction of tryptophan at the amino acid 85 position. In addition to disruption of direct interactions with DNR1, the Arg85Trp variant can also be predicted to impact the overall structure of HNF4α by altering the organization of LBD and DBD parts in the homodimer.

Histology

Histology of the liver showed complete porto-portal bridging cirrhosis with limited inflammation around the portal fields and septa (Fig. 4). Glycogen granules were also observed.

Histology of the kidney (HE staining) showed normal cellularity, normal basement membrane, and some erythrocytes in slightly ectatic capillaries (focal and segmental distribution). Normal proximal tubule cells, arteries, and arterioles were observed. Glomerular immunohistochemistry showed focal as well as segmental, irregular positivity (+) for IgM (normal for IgG, IgA, C5b-9, C3C, fibrinogen, and C4d). Tubular immunohistochemistry showed a focus-like positivity (+) for albumin and IgG (data not shown). Mild type 2 fiber atrophy was observed in the skeletal muscle biopsy (data not shown).

Liver and kidney mitochondria were evaluated by electron microscopy. Most of the liver mitochondria were considered unremarkable, apart from a few that were very large (diameter approx. 4μm, norm: 1μm) and brighter in appearance. The mitochondria in the kidney glomeruli appeared unremarkable. In contrast, the mitochondria of the tubule cells showed strongly pronounced cristae and a broad spectrum of shapes. Areas showing densely placed and circularly shaped mitochondria were adjacent to areas of mainly large and irregularly shaped mitochondria in a smaller number (Fig. 5).

Quantification of glycogen in homogenized liver tissue showed a slightly increased glycogen level (7.5g/100 g, norm: 2.4–6.4 g, mean: 4.6 g), as well as increased protein content (Lowry, 613 mg/g, norm: 141–226 mg, mean: 181 mg). Evidence of GLUT-2 expression in the liver was detected by immunohistochemistry (data not shown).

Mitochondrial Function

Functional investigations were carried out on the biopsies (Table 3). Apart from borderline decreased citrate synthase activity in liver tissue, which is suggestive of a low number of mitochondria, OXPHOS activity in liver homogenate, skeletal muscle, and fibroblasts was normal. Respirometric analysis of intact mitochondria showed a slight decrease in succinate-dependent respiration, resulting in an increase of the succinate-related pyruvate respiration in muscle cells, indicative of a reduced complex II-dependent respiration.

Discussion

Molecular Level

The two promoters responsible for HNF4α transcription are expressed in a time- and tissue-specific manner: P1-derived isoforms (HNF4α 1–6) are found in the adult liver and kidney, whereas P2-derived isoforms (HNF4α 7–12) are mainly expressed in the pancreas, bile duct, intestine, and fetal liver. Although HNF4α exclusively dimerizes with itself, Ko et al. [2019] showed that additional combinatorial isoform-heterodimers activate distinctive target genes, leading to the increased functional diversity of HNF4α [Ko et al., 2019]. The DBD region of HNF4α is highly conserved across species; thus, in sequence alignment from different species, no substitutions to arginine 85 were observed (data not shown). Our structural analysis predict an overall negative impact on DNA binding and recognition since the variant lies in the DBD.

Additionally, our structural analysis shows that the variant may change the protein's overall structure by

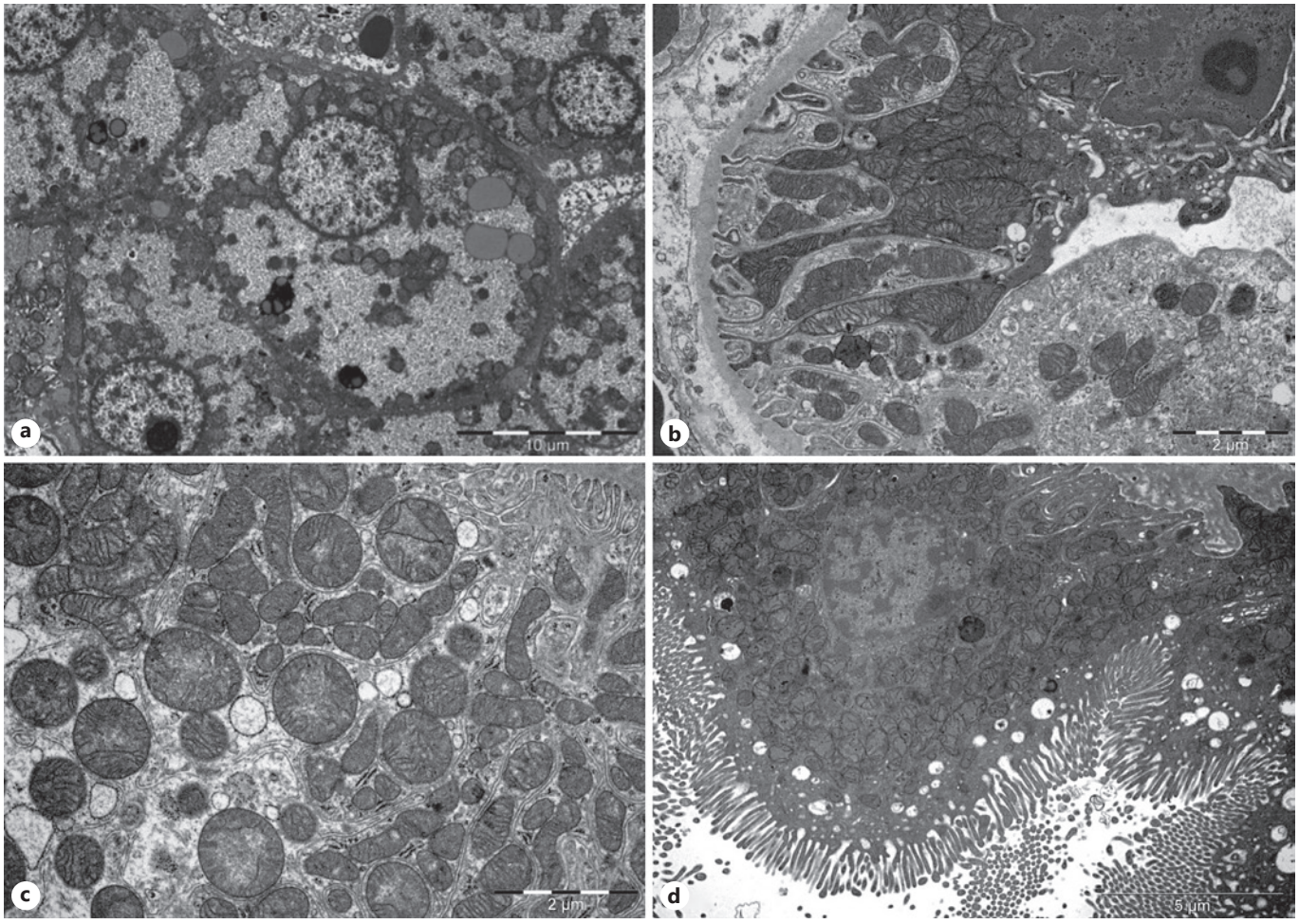

Fig. 5. EM pictures from biopsies performed at age of 5 years. **a** Overview of a normal hepatocyte. **b** Overview of the distal tubule. Showing damaged mitochondria. **c** Distal tubule with circularly shaped mitochondria. **d** Proximal tubule of the kidney.

altering the organization of the LBD and DBD. During the reorganization of LBD and DBD, the position of the p.(Arg85Trp) variant within the DBD can impact the function of HNF4α at the following levels: homodimerization and heterodimerization of isoforms, binding affinity to target genes, interference with the regulatory phosphorylation of serine at position 87 and the network to other TFs. Furthermore, the change in the structure of the DBD may also change the DNA sequence recognized [Hamilton et al., 2014]. This change could result in the altered regulation of a new set of genes. Thus, the different amino acid (tryptophan instead of arginine) at this position in the DBD causes an altered DNA binding, which may lead to either a simple loss-of-function, a dominant-negative effect or to completely novel targets (i.e. gain-of-function effect) of the mutant protein, as well as in a combination of these. Further molecular studies are needed to elucidate the details.

Organ Level

It has been shown that HNF4α reprograms α-cells to β-cells in the pancreas; therefore, HNF4α is essential for beta-cell function and morphology [Sangan et al., 2015]. For example, the glucose-regulated secretion of insulin seems to be HNF4α-dependent; however, the precise molecular mechanism remains elusive [Gupta et al., 2005; Miura et al., 2006]. The increased insulin concentration in utero and its growth-stimulating actions during the fetal period explain the macrosomia in patients with the p.(Arg85Trp) variant [Kapoor et al., 2008]. The *KCNJ11* gene, coding for the Kir6.2 subunit of the ATP-potassium

Table 3. OXPHOS activity and oxygraphy of the patient

	Skin fibroblasts	Liver homogenate	Skeletal muscle
OXPHOS activity			
Complex I mU/mU CS	0.34 (0.19–0.46)	0.70 (0.28–0.83)	0.21 (0.14–0.28)
Complex II mU/mU CS	0.32 (0.17–0.52)	1.32 (0.59–2.14)	0.18 (0.14–0.36)
Complex III mU/mU CS	0.48 (0.35–0.87)	1.66 (0.54–2.14)	0.70 (0.5–1.11)
Complex IV mU/mU CS	0.54 (0.42–1.11)	2.39 (0.91–3.3)	0.97 (0.57–1.76)
Complex V mU/mU CS	0.24 (0.12–0.38)	0.95 (0.25–1.1)	0.38 (0.17–0.66)
CS mU/mg protein	189 (134–228)	**21** (22–41)	147.5 (70–173)
Oxygraphy (muscle biopsy)			
Active O_2 flow referred to pyruvate, pmol/(s*mg)			19 (12–22)
Active O_2 flow referred to succinate, pmol/(s*mg)			**11** (12–20)
Maximal coupled respiration (pyruvate and succinate as the substrate), pmol/(s*mg)			29 (20–33)
Maximal uncoupled respiration (pyruvate, succinate, FCCP), pmol/(s*mg)			35 (22–39)
Complex IV respiration, pmol/(s*mg)			39 (26–64)
SRPR (quotient of pyruvate/succinate respiration)			**1.52** (0.91–1.42)
Flux control ratio 1			0.59 (0.49–0.61)
Flux control ratio 2			0.86 (0.81–0.96)
Flux control ratio 3			0.41 (0.39–0.63)

Table showing the results of the OXPHOS activities and oxygraphy measurements. Reference values in parentheses. CS, citrate synthase; SRPR, succinate-related pyruvate respiration. Bold, values outside reference ranges.

channel, is a target gene of HNF4α. However, hyperinsulinism due to HNF4A deficiency is typically responsive to already low doses of diazoxid, which blocks this channel in the open state. Thus, the presence of a functional potassium channel is needed for this treatment to work. Many types of hyperinsulinism taper off during childhood, regardless of the molecular mechanism. Patients may develop MODY1 later on, as reported in previous studies on three patients aged 12, 13, and 20 years [Liu et al., 2018; Sheppard et al., 2020].

Ferrer et al. [2002] showed a cross regulatory network of HNF4α and HNF1α in beta cells of the pancreas with equilibrium states, in which a decrease in expression of one automatically leads to a decrease of the other TFs [Ferrer, 2002]. Consequently, it is not surprising that the MODY1 (HNF4A variant-related) and MODY3 (HNF1A variant-related) share some clinical features (dual type: first congenital hyperinsulinism [CHI], later diabetes) [Galcheva et al., 2019]. So far, our patient has no sign of diabetes, including normal HbA1C levels.

This pathogenic variant causes hepatomegaly and an increase in glycogen content. One patient has been reported with mild portal inflammation and fibrosis [Stanescu et al., 2012]. Our patient additionally showed liver cirrhosis that remained stable over time, whereas a gradual decrease of AST and ALT to practically normal values by age 7 years was observed. The timeline of the two promoter's differential activation may be essential here: there is a switch from promoter P2 in the fetal liver to P1 in the adult liver, possibly in the context of a potentially less pro-inflammatory milieu. However, it is not known at what age this switch occurs in humans.

Since the network of TFs is different in fetal and adult hepatocytes, it is obvious that the function of HNF4α, as a master regulator of the hepatocytes, varies among different time stages of development [Lau et al., 2018]. Figure 1 illustrates that in most reported patients, clinical symptoms change during development. Most patients initially presented with macrosomia, CHI, and hepatomegaly and showed stabilization of these symptoms in parallel with a progression of the subsequent Fanconi-type proximal tubulopathy. Our case strengthens this observation in two aspects: first, the vanishing of the hyperinsulinism and second, the decrease of liver enzymes both happen around the same time, in our patient at age 7 years. The change of symptoms over time is suggesting different functions of HNF4α depending on age. Around the age of 7 years, many physiological changes can be observed in children and various factors have an influence on these. Additionally, the switch of promoters might also contribute to the major physiological transition observed in patients with the p.(Arg85Trp) variant. However, based on the data of our patient, we are not able to conclusively differentiate between an age-related pene-

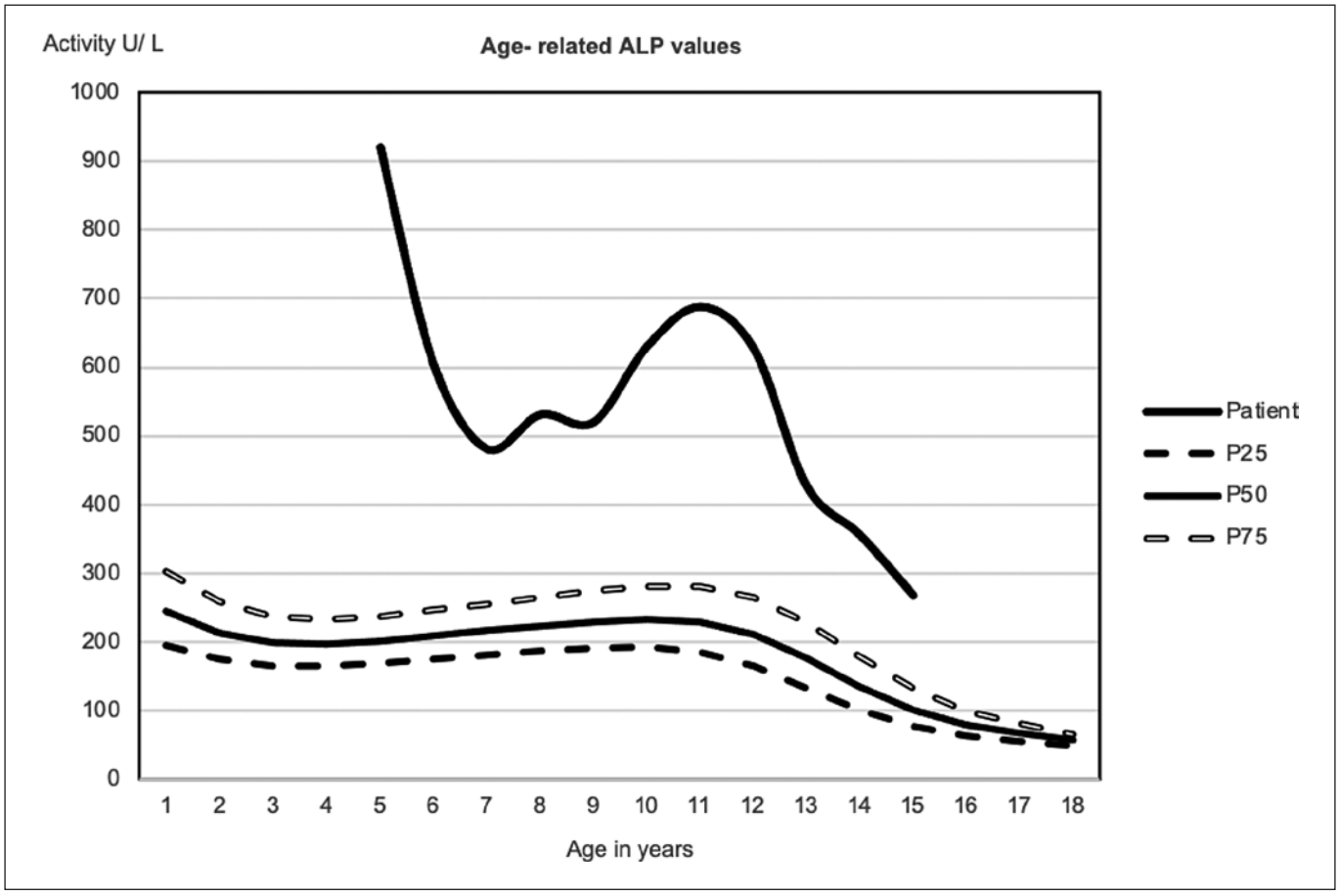

Fig. 6. Age-related ALP levels of the patient compared to normal levels. Reference values (extracted from Zierk et al. [2017]) are presented in three centile curves: P25, P50, and P75. No data before age 5 years. ALP, alkaline phosphatase.

trance of symptoms versus a change of HNF4α functions over time including the hypothesis of a switch of promoters. This suggested disease mechanism will need to be substantiated by further evidence.

In the kidney, the variant causes a proximal tubulopathy resulting in Fanconi syndrome. The Fanconi syndrome is characterized by glucosuria, low-weight proteinuria, hypercalciuria, phosphaturia, and bicarbonate loss, resulting in renal tubular acidosis [Foreman, 2019]. Our patient had nephrocalcinosis, which is also described in other patients carrying the variant [Liu et al., 2018]. Experiments with Hnf4α-knockout mice showed that Hnf4α seems to be necessary for the proximal tubule formation and the regulation of proximal tubule-specific genes. This results in a lower density of transporters in each tubule cell and a deformation of proximal tubule cells [Marable et al., 2018]. If this also applies to humans, it could explain the proximal tubulopathy. The p.(Arg85Trp) is the only variant showing renal impact compared to other variants within the DBD [Hamilton et al., 2014]. Thus, a common loss-of-function effect appears, not to explain the specific impact on the proximal tubular function sufficiently; instead, we hypothesize that the above-described gain-of-function concept could be applicable to this issue. In contrast to the proximal tubulopathy observed in most patients, CKD is only described in one other patient [Anyiam et al., 2019]. Our patient's histology also exhibited segmental glomerular changes, suggestive of a glomerular component impacting her kidney.

Further research is needed, not only on the direct effects of the variant on the glomeruli but also on the differences in appearance and clinical severity between proximal tubulopathy and CKD among patients with this

variant. The complex metabolic condition and the proximal tubulopathy are risk factors for poor bone health. Although serum phosphate and calcium levels were always normal, the proximal tubulopathy led to increased urinary loss of calcium and phosphate; the latter is reflected by a low TRP. Thus, our patient developed mixed calcipenic and phosphopenic rickets at 5 years of age. The high levels of ALP and the increased β-cross laps are consistent with this diagnosis. Due to the high levels of ALP, we investigated the different isoforms of ALP in our patient, finding only the bone-specific ALP to be elevated (data not shown). The normal bone density at 8 years of age suggested that the treatment was efficient. The persistently increased ALP levels between age 10 and 14 years suggested that more aggressive treatment may be needed (Fig. 6). Thus, cholecalciferol was added to the treatment regimen (at age 15.5 years) with the aim to normalize the ALP levels without increasing the calciuria.

Metabolic Level

Hamilton et al. [2014] showed that patients with the p.(Arg85Trp) variant had elevated serum magnesium levels parallel to increased urine levels. The serum level only represents 1% of the total magnesium, but the higher serum levels could be a sign of disruption of magnesium homeostasis through increased dissolution from storage organs, resulting in magnesium deficiency in the long run. A generalized magnesium deficiency seems unlikely, based on two observations: First, the peripheral quantitative computed tomography measurement of the distal radius showed no indirect signs of a magnesium deficiency. Second, the patient never had symptoms of magnesium deficiency. Muscle pain experienced during childhood resolved sometime after treating the rickets but without normalization of serum magnesium.

Patients with the p.(Arg85Trp) variant show low serum urate levels, possibly due to tubulopathy. This is supported by the fact that other *HNF4A* variants, which do not affect the kidneys, show normal serum urate levels [Hamilton et al., 2014]. Direct effects of HNF4α on the transcription of urate transporters, including PDZK1 [Ketharnathan et al., 2018] and SLC2A9 [Prestin et al., 2014], have been observed. However, the effects on the transporters and the contribution to the low serum levels of urate remain elusive. Interestingly, low urate levels are also commonly seen in patients with glycogen storage disease. It is known that HNF4α regulates both the expression of genes of the gluconeogenesis [Chavalit et al., 2013] and glycolytic enzymes (aldolase B, glyceraldehyde-3-phosphate dehydrogenase, and liver pyruvate kinase) [Stoffel and Duncan, 1997]. The increased glycogen content in the liver of patients with the variant is still not fully understood. In our patient, this increased glycogen storage together with proximal tubulopathy led to the differential diagnosis of Fanconi-Bickel syndrome. It is known that the GLUT-2 gene (*SLC2A2*) is a target gene of HNF1α. It can be hypothesized that HNF4α has an indirect impact via HNF1α [Stanescu et al., 2012; Sheppard et al., 2020]. The GLUT-2 expression in the liver was preserved in our patient, but we do not know if the amount, or the activity, was decreased. Taken all these clinical (e.g., frontal bossing, see above), histological, and biological findings together, this variant-specific HNF4A defect may be considered a new type of glycogen storage disease.

Since HNF4α is a crucial regulator of hepatic lipid metabolism, Hnf4α-knockout mice have reduced levels of apolipoproteins combined with lower VLDL secretion, lipogenesis, and de novo cholesterol synthesis [Yin et al., 2011]. Lab values of the blood lipids in a patient with the p.(Arg85Trp) variant are presented here for the first time (Table 1). The apolipoproteins were normal at 15 years (data not shown). We do not know whether they were always normal or increased simultaneously with the HDL's increase (at age 7 years). Studies on lipid metabolism in drosophila revealed an interesting model for the impact of HNF4α on lipid metabolism and fatty acid oxidation. Palanker et al. [2009] proposed that the absence of the dietary fatty acids of triglycerides could directly, or indirectly, activate HNF4α, whose target genes then promote beta-oxidation in mitochondria [Palanker et al., 2009]. Since the metabolism of our patient was kept anabolic during the first years, with strict short fasting periods, this could be the reason why the impact of the variant on the lipid metabolism may not be as visible as it would be in a catabolic state. Marchesin et al. [2019] studied the p.(Arg85Trp) variant in nephrocytes of drosophila and showed a decrease of genes for mitochondrial structure and functions, followed by a reduction of beta-oxidation, which led to an accumulation of lipid droplets [Marchesin et al., 2019].

Our patient showed impaired succinate-dependent respiration in muscle (Table 3), but we do not have any evidence for impaired beta-oxidation, either in acylcarnitines or urinary organic acids (data not shown). She showed only an intermittent increase of Krebs cycle intermediates in urinary organic acids, consistent with an expected functional impairment of the mitochondria in the kidneys related to their high energy needs. Our patient also showed abnormal mitochondrial morphology. This change appeared to be much more pronounced in

the kidney than in the liver and potentially could be secondary to the impaired energy metabolism, rather than caused by the variant directly.

HNF4α has a significant role in the inflammation process. Cytokines (e.g., IL-1 and TGF-beta can increase or decrease HNF4α expression in different inflammatory contexts) modulate the binding activity of HNF4α and the induced target genes that, in turn, regulate cytokines and inflammation pathways (e.g., NF-KB) [Babeu and Boudreau, 2014]. A clinical panel for the levels of the inflammatory mediators IL-1, IL-6, IL-10, IL-12, and TNFα, was performed at age 15.5 years and was within a normal range (data not shown). Since the clinical panel was not performed until age 15.5 years, we can only speculate about a pro-inflammatory milieu due to the variant.

Nevertheless, we have hints for an inflammatory process in the liver: the low HDL and increased ferritin (data not shown), combined with the early appearance of the liver cirrhosis in our patient and the portal inflammation described in another patient [Stanescu et al., 2012] might be the consequence of a (past) inflammatory process in the liver. HNF1α is a significant regulator of glucose and lipid metabolism and is essential in the inflammation network. However, indirect effects of HNF4α on pathways, such as in the glucose metabolism, cannot be excluded. Liver cirrhosis has been described in only one other patient [Stanescu et al., 2012]; therefore, further research is needed on the mechanism behind the change in the pro-inflammatory milieu caused by HNF4α deficiency.

Conclusion

Our patient expands the variant-specific phenotype of the p.(Arg85Trp) variant, showing hepatic glycogen storage features and cirrhosis, impaired mitochondrial morphology and function, disruption of the lipoprotein metabolism, and glomerular changes. A major physiological transition during childhood, including the stabilization, or even disappearance, of the CHI, liver involvement (hepatomegaly, increased liver enzymes), and lipoprotein metabolism parallel to a progression of the subsequent Fanconi-type proximal tubulopathy had been observed. Further research is needed to verify our hypotheses regarding the disease mechanism and to better understand the full scope of effects of the p.(Arg85Trp) variant of *HNF4A*. This will help to improve our understanding of the important role of HNF4α in human development and physiology.

Acknowledgments

We thank the patient and her family for kindly agreeing to this publication; Prof B. Thorrens (Lausanne) for immunohistochemistry of GLUT-2; Dr. Patricie Burda (Zürich) for glycogen quantification in liver homogenate; Dr. Matteo Montani (Bern) for his help with liver histology; J. and M. Winkler, C. Schmutz, and M. Grassi for linguistic advice.

Statement of Ethics

Written informed consent was obtained from the patient and her parents for publication of the details of her medical case, accompanying data and investigations. Ethical approval was not required for this study in accordance with local and national regulations.

Conflict of Interest Statement

The authors have no conflicts of interest to declare.

Funding Sources

No funding was provided for this study.

Author Contributions

Mara Grassi designed the study, collected the data, and wrote the first draft of the study. This study was performed as a thesis to be submitted in partial fulfillment of the requirements for the degree of a medical doctor. Bernard Laubscher followed up the patient, contributed to the study design and collection of data, and critically revised the manuscript. Amit V. Pandey performed the sequence and structure analysis of HNF4a. He contributed to writing and gave important conceptual input to the manuscript. Sibylle Tschumi was the attending nephrologist and collected and analyzed the data of renal function. She contributed to writing and critically reviewing the manuscript. Franziska Graber produced the electron microscopy images of liver and kidney biopsies and contributed to their analyses and interpretation. She critically revised the manuscript. André Schaller performed and interpreted the whole-genome sequencing, contributed to interpretation of the data, and critically revised the manuscript. Marco Janner and Daniel Aeberli were involved in the treatment and follow-up of bone metabolism, the corresponding interpretation of data, and critical revision of the manuscript. Ekkehard Hewer was involved in the supervision of pathological analyses and interpretation of data. He critically revised the manuscript. Jean-Marc Nuoffer carried out and interpreted the mitochondrial analyses. He contributed important intellectual content and critically revised the manuscript. He was also the supervisor of the MD thesis. Matthias Gautschi was attending physician of the patient, designed the study, contributed to the collection and interpretation of data, and critically revised the manuscript. He was the co-advisor of Mara Grassi.

Data Availability Statement

All data were extracted from protected clinical databases (apart from the in silico analyses of the sequence and structure of HNF4α, which were produced with publicly available tools as described in the investigations section). Founded and specific requests for source data may be directed to the corresponding author.

References

Anyiam O, Wallin E, Kaplan F, Lawrence C. A complicated pregnancy in an adult with HNF4A p.R63W-associated Fanconi syndrome. Case Rep Med. 2019;2019:1–5.

Babeu J-P, Boudreau F. Hepatocyte nuclear factor 4-alpha involvement in liver and intestinal inflammatory networks. World J Gastroenterol. 2014;20(1):22–30.

Canutescu AA, Shelenkov AA, Dunbrack RL. A graph-theory algorithm for rapid protein side-chain prediction. Protein Sci. 2003;12(9):2001–14.

Chandra V, Huang P, Potluri N, Wu D, Kim Y, Rastinejad F. Multidomain integration in the structure of the HNF-4α nuclear receptor complex. Nature. 2013;495(7441):394–8.

Chavalit T, Rojvirat P, Muangsawat S, Jitrapakdee S. Hepatocyte nuclear factor 4α regulates the expression of the murine pyruvate carboxylase gene through the HNF4-specific binding motif in its proximal promoter. Biochim Biophys Acta. 2013;1829(10):987–99.

Clemente M, Vargas A, Ariceta G, Martínez R, Campos A, Yeste D. Hyperinsulinaemic hypoglycaemia, renal Fanconi syndrome and liver disease due to a mutation in the HNF4A gene. Endocrinol Diabetes Metab Case Rep. 2017;2017(1):16-0133.

Duan Y, Wu C, Chowdhury S, Lee MC, Xiong G, Zhang W, et al. A point-charge force field for molecular mechanics simulations of proteins based on condensed-phase quantum mechanical calculations. J Comput Chem. 2003;24(16):1999–2012.

Fang B, Mane-Padros D, Bolotin E, Jiang T, Sladek FM. Identification of a binding motif specific to HNF4 by comparative analysis of multiple nuclear receptors. Nucleic Acids Res. 2012;40(12):5343–56.

Ferrer JA. A genetic switch in pancreatic beta-cells: implications for differentiation and haploinsufficiency. Diabetes. 2002;51(8):2355–62.

Foreman JW. Fanconi syndrome. Pediatr Clin North Am. 2019;66(1):159–67.

Galcheva S, Demirbilek H, Al-Khawaga S, Hussain K. The genetic and molecular mechanisms of congenital hyperinsulinism. Front Endocrinol. 2019;10:111.

Geary DF, Schaefer F. Comprehensive pediatric nephrology. In: Comprehensive Pediatric Nephrology. 1st ed. Mosby; 2008. p. 4.

Gnaiger E. Mitochondrial pathways and respiratory control: an introduction to OXPHOS analysis. 5th ed. Bioenerg Commun; 2020. p. 2.

Gupta RK, Vatamaniuk MZ, Lee CS, Flaschen RC, Fulmer JT, Matschinsky FM, et al. The MODY1 gene HNF-4alpha regulates selected genes involved in insulin secretion. J Clin Invest. 2005;115(4):1006–15.

Hamilton AJ, Bingham C, McDonald TJ, Cook PR, Caswell RC, Weedon MN, et al. The HNF4A R76W mutation causes atypical dominant Fanconi syndrome in addition to a β cell phenotype. J Med Genet. 2014;51(3):165–9.

Harries LW, Locke JM, Shields B, Hanley NA, Hanley KP, Steele A, et al. The diabetic phenotype in HNF4A mutation carriers is moderated by the expression of HNF4A isoforms from the P1 promoter during fetal development. Diabetes. 2008;57(6):1745–52.

Improda N, Shah P, Güemes M, Gilbert C, Morgan K, Sebire N, et al. Hepatocyte nuclear factor-4 alfa mutation associated with hyperinsulinaemic hypoglycaemia and atypical renal Fanconi syndrome: expanding the clinical phenotype. Horm Res Paediatr. 2016;86(5):337–41.

Jorgensen WL, Chandrasekhar J, Madura JD, Impey RW, Klein ML. Comparison of simple potential functions for simulating liquid water. J Chem Phys. 1983;79(2):926–35.

Kapoor RR, Locke J, Colclough K, Wales J, Conn JJ, Hattersley AT, et al. Persistent hyperinsulinemic hypoglycemia and maturity-onset diabetes of the young due to heterozygous HNF4A mutations. Diabetes. 2008;57(6):1659–63.

Ketharnathan S, Leask M, Boocock J, Phipps-Green AJ, Antony J, O'Sullivan JM, et al. A non-coding genetic variant maximally associated with serum urate levels is functionally linked to HNF4A-dependent PDZK1 expression. Hum Mol Genet. 2018;27(22):3964–73.

Ko HL, Zhuo Z, Ren EC. HNF4α combinatorial isoform heterodimers activate distinct gene targets that differ from their corresponding homodimers. Cell Rep. 2019;26(10):2549–57.e3.

Krieger E, Vriend G. New ways to boost molecular dynamics simulations. J Comput Chem. 2015;36(13):996–1007.

Lau HH, Ng NHJ, Loo LSW, Jasmen JB, Teo AKK. The molecular functions of hepatocyte nuclear factors: in and beyond the liver. J Hepatol. 2018;68(5):1033–48.

Lausen J, Thomas H, Lemm I, Bulman M, Borgschulze M, Lingott A, et al. Naturally occurring mutations in the human HNF4alpha gene impair the function of the transcription factor to a varying degree. Nucleic Acids Res. 2000;28(2):430–7.

Lemaire M. Novel Fanconi renotubular syndromes provide insights in proximal tubule pathophysiology. Am J Physiol Ren Physiol. 2021;320(2):F145–60.

Liu J, Shen Q, Li G, Xu H. HNF4A-related Fanconi syndrome in a Chinese patient: a case report and review of the literature. J Med Case Rep. 2018;12(1):203.

Marable SS, Chung E, Adam M, Potter SS, Park JS. Hnf4a deletion in the mouse kidney phenocopies Fanconi renotubular syndrome. JCI Insight. 2018;3(14):e97497.

Marchesin V, Pérez-Martí A, Le Meur G, Pichler R, Grand K, Klootwijk ED, et al. Molecular basis for autosomal-dominant renal Fanconi syndrome caused by HNF4A. Cell Rep. 2019;29(13):4407–21.e5.

Miura A, Yamagata K, Kakei M, Hatakeyama H, Takahashi N, Fukui K, et al. Hepatocyte nuclear factor-4alpha is essential for glucose-stimulated insulin secretion by pancreatic beta-cells. J Biol Chem. 2006;281(8):5246–57.

Numakura C, Hashimoto Y, Daitsu T, Hayasaka K, Mitsui T, Yorifuji T. Two patients with HNF4A-related congenital hyperinsulinism and renal tubular dysfunction: a clinical variation which includes transient hepatic dysfunction. Diabetes Res Clin Pract. 2015;108(3):e53–5.

Palanker L, Tennessen JM, Lam G, Thummel CS. Drosophila HNF4 regulates lipid mobilization and β-oxidation. Cell Metab. 2009;9(3):228–39.

Pearson ER, Pruhova S, Tack CJ, Johansen A, Castleden HAJ, Lumb PJ, et al. Molecular genetics and phenotypic characteristics of MODY caused by hepatocyte nuclear factor 4alpha mutations in a large European collection. Diabetologia. 2005;48(5):878–85.

Pearson ER, Boj SF, Steele AM, Barrett T, Stals K, Shield JP, et al. Macrosomia and hyperinsulinaemic hypoglycaemia in patients with heterozygous mutations in the HNF4A gene. PLoS Med. 2007;4(4):e118.

Prestin K, Wolf S, Feldtmann R, Hussner J, Geissler I, Rimmbach C, et al. Transcriptional regulation of urate transportosome member SLC2A9 by nuclear receptor HNF4α. Am J Physiol Ren Physiol. 2014;307(9):F1041–51.

Rauch F, Schöenau E. Peripheral quantitative computed tomography of the distal radius in young subjects: new reference data and interpretation of results. J Musculoskelet Neuronal Interact. 2005;5(2):119–26.

Renner K, Amberger A, Konwalinka G, Kofler R, Gnaiger E. Changes of mitochondrial respiration, mitochondrial content and cell size after induction of apoptosis in leukemia cells. Biochim Biophys Acta. 2003;1642(1-2):115–23.
Sangan CB, Jover R, Heimberg H, Tosh D. In vitro reprogramming of pancreatic alpha cells towards a beta cell phenotype following ectopic HNF4α expression. Mol Cell Endocrinol. 2015;399:50–9.
Schaller A, Hahn D, Jackson CB, Kern I, Chardot C, Belli DC, et al. Molecular and biochemical characterisation of a novel mutation in POLGassociated with Alpers syndrome. BMC Neurol. 2011;11(1):4.
Shepherd D, Garland PB. The kinetic properties of citrate synthase from rat liver mitochondria. Biochem J. 1969;114(3):597–610.
Sheppard SE, Barrett B, Muraresku C, McKnight H, De Leon DD, Lord K. Heterozygous recurrent HNF4A variant p.Arg85Trp causes Fanconi renotubular syndrome 4 with maturity onset diabetes of the young, an autosomal dominant phenocopy of Fanconi Bickel syndrome with colobomas. Am J Med Genet A. 2021;185(2):566–70.
Stanescu DE, Hughes N, Kaplan B, Stanley CA, De León DD. Novel presentations of congenital hyperinsulinism due to mutations in the MODY genes: HNF1A and HNF4A. J Clin Endocrinol Metab. 2012;97(10):E2026–30.
Stoffel M, Duncan SA. The maturity-onset diabetes of the young (MODY1) transcription factor HNF4alpha regulates expression of genes required for glucose transport and metabolism. Proc Natl Acad Sci U S A. 1997;94(24):13209–14.
Thomas H, Jaschkowitz K, Bulman M, Frayling TM, Mitchell SM, Roosen S, et al. A distant upstream promoter of the HNF-4alpha gene connects the transcription factors involved in maturity-onset diabetes of the young. Hum Mol Genet. 2001;10(19):2089–97.
Wallerman O, Motallebipour M, Enroth S, Patra K, Bysani MSR, Komorowski J. Molecular interactions between HNF4a, FOXA2 and GABP identified at regulatory DNA elements through ChIP-sequencing. Nucleic Acids Res. 2009;37(22):7498–508.
Walsh SB, Unwin R, Kleta R, van't Hoff W, Bass P, Hussain K, et al. Fainting Fanconi syndrome clarified by proxy: a case report. BMC Nephrol. 2017;18(1):230.
Yin L, Ma H, Ge X, Edwards PA, Zhang Y. Hepatic hepatocyte nuclear factor 4α is essential for maintaining triglyceride and cholesterol homeostasis. Arterioscler Thromb Vasc Biol. 2011;31(2):328–36.
Zemel BS, Stallings VA, Leonard MB, Paulhamus DR, Kecskemethy HH, Harcke HT. Revised pediatric reference data for the lateral distal femur measured by hologic discovery/delphi dual-energy X-ray absorptiometry. J Clin Densitom. 2009;12(2):207–18.
Zierk J, Arzideh F, Haeckel R, Cario H, Fruhwald MC, Gros HJ, et al. Pediatric reference intervals for alkaline phosphatase. Clin Chem Lab Med. 2017;55(1):102–10.